

# Technical Notes

TECHNICAL NOTES are short manuscripts describing new developments or important results of a preliminary nature. These Notes cannot exceed 6 manuscript pages and 3 figures; a page of text may be substituted for a figure and vice versa. After informal review by the editors, they may be published within a few months of the date of receipt. Style requirements are the same as for regular contributions (see inside back cover).

## Effects of Turbulence Model Constants on Computation of Confined Swirling Flows

J. M. Khodadadi\* and N. S. Vlachos†  
University of Illinois at Urbana-Champaign,  
Urbana, Illinois

### Introduction

PREDICTION of the detailed behavior of confined swirling flows is of great importance in improving the performance of gas turbine combustors and cyclone chambers. The objective of the present work was to systematically assess the applicability of the standard  $k-\epsilon$  turbulence model and one of its variations to predict decaying swirl in developing turbulent pipe flow. This particular flowfield was selected to minimize numerical diffusion, thus allowing assessment of the physical model. The experimental study of Weske and Sturov,<sup>1</sup> which provides detailed inlet measurements for the axial and tangential velocity profiles, and turbulence kinetic energy, was chosen for comparison purposes.

### Computational Technique

The present work utilizes the SIMPLE procedure of Patankar.<sup>2</sup> The elliptic equations governing this problem are of the general form

$$\frac{\partial}{\partial z}(\rho U \phi) + \frac{1}{r} \frac{\partial}{\partial r}(\rho r V \phi) = \frac{\partial}{\partial z} \left( \Gamma_{\phi} \frac{\partial \phi}{\partial z} \right) + \frac{1}{r} \frac{\partial}{\partial r} \left( \Gamma_{\phi} r \frac{\partial \phi}{\partial r} \right) + S_{\phi} \quad (1)$$

where  $U$  and  $V$  represent the time-averaged velocities in the axial ( $z$ ) and radial ( $r$ ) directions, respectively. Because of space limitations, the various transport equations are not listed here, but can be found in Ref. 3. The standard  $k-\epsilon$  turbulence model used for the present computations was suggested by Launder and Spalding.<sup>4</sup> Abujelala and Lilley<sup>5</sup> recently proposed adjusting three constants in the  $k-\epsilon$  model when applied to confined swirling flows. The new values were determined by minimizing the difference between computations and turbulence measurements in a flow configuration involving a swirling jet discharging into a sudden expansion. The recom-

mended constants were

$$C_{\mu} = 0.125, \quad C_2 = 1.5942, \quad \sigma_{\epsilon} = 1.1949 \quad (2)$$

which differ from the "standard" constants<sup>4</sup>

$$C_{\mu} = 0.09, \quad C_2 = 1.92, \quad \sigma_{\epsilon} = 1.22 \quad (3)$$

A schematic of the geometry of swirling flow in a pipe is shown in Fig. 1. The boundary conditions imposed were those of standard practice in numerical computations. At the outlet station, which was placed 160 pipe diameters downstream of the inlet plane, the flow was assumed to be fully developed. The radial velocity and normal gradients of other variables were set to zero at the symmetry axis. Standard log-law wall functions were used for the next-to-the-wall grid points.<sup>4</sup> The study of Weske and Sturov<sup>1</sup> ( $Re = U_m D / \nu = 3 \times 10^5$ ) provided detailed inlet measurements for  $U$ ,  $W$ , and  $k$ , which were used as boundary conditions for the computations. The variation of  $\epsilon$  at the inlet plane was set to  $k^{1.5}/(0.01R)$ . The swirl number at the inlet plane was determined from

$$S = \int_0^R (Wr) \rho U 2\pi r dr / R \int_0^R U \rho U 2\pi r dr \quad (4)$$

and the measured values of  $U$  and  $W$ .

The extent and dominance of numerical diffusions for this geometry was assessed in Refs. 3 and 6. A  $24 \times 25$  grid, which accommodated both memory-size limitations and tolerable numerical diffusion, was chosen for final production runs. Expanding grids were employed in the streamwise direction and away from the wall. Staggered control volumes were used for the axial and radial velocity components. All other quantities of interest, including the tangential velocity component, were computed at the grid points. The finite-difference forms of the time-averaged transport equations were obtained by adopting a semi-integral approach to discretize the equations over each control volume of the computational grid by using a hybrid-difference scheme. The line-by-line method was used to obtain converged solutions iteratively, whereas relaxation factors were employed to promote stability of the process. These factors were 0.3, 0.2, 0.45, 0.8, and 0.8 for  $U$ ,  $V$ ,  $W$ ,  $k$ , and  $\epsilon$ , respectively. Other details of the computational method and convergence characteristics can be found in Refs. 3 and 6.

### Results and Discussion

Comparison of the computed and measured axial velocity component is presented in Fig. 2 for  $S = 1.445$ . The measured inlet profile for the  $U$  velocity ( $z/D = 0.35$ ) is seen in Fig. 2 and, undoubtedly, is very different from a uniform profile. Two sets of computations are presented, with the solid line representing the standard  $k-\epsilon$  model and the dashed line representing the modified  $k-\epsilon$  of Ref. 5. In general, the agreement of the measurements with the computations is good and the evolution of the  $U$  velocity profiles is well predicted, except near the symmetry axis for the  $z/D = 20$  and 50 stations, where the measurements are consistently below both sets of computations. The results obtained with the modified model are lower than the standard model near the symmetry axis and are higher than the standard model near the wall for

Received July 8, 1988; revision received Feb. 7, 1989. Copyright © 1989 American Institute of Aeronautics and Astronautics, Inc. All rights reserved.

\*Graduate Student, Department of Mechanical and Industrial Engineering; currently Assistant Professor, Department of Mechanical Engineering, Auburn University, Auburn, AL. Member AIAA.

†Assistant Professor, Department of Mechanical and Industrial Engineering; currently Senior Manager, CHAM of North America, Inc., Huntsville, AL. Member AIAA.

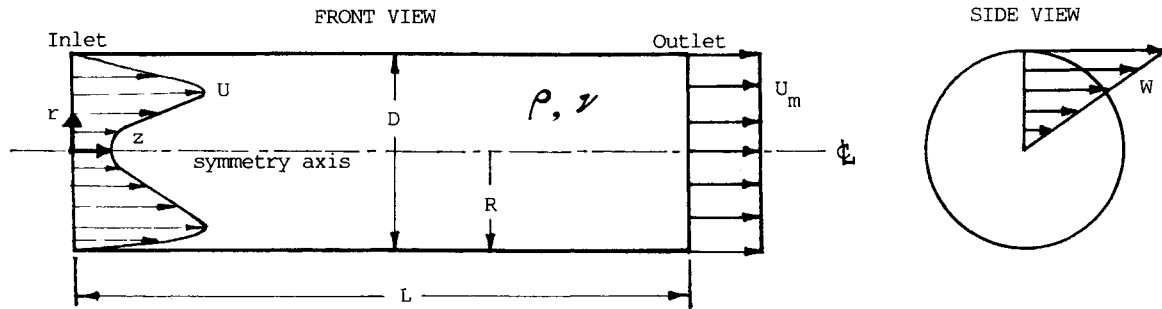


Fig. 1 Schematic of swirling flow in a pipe.

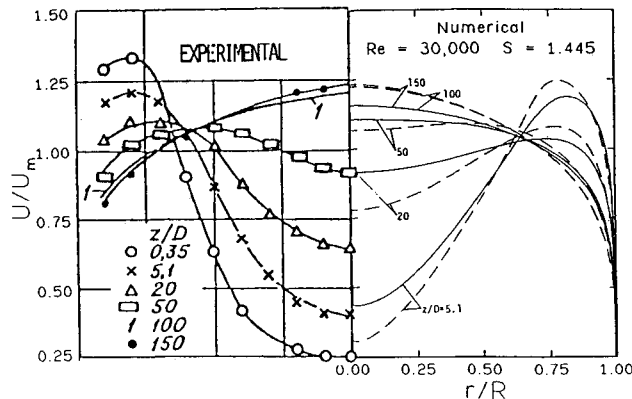


Fig. 2 Mean axial velocity profiles.

$z/D = 5.1, 20$ , and  $50$ . This effect is reversed for the profiles at  $z/D = 100$  and  $150$ . It is clear that the measured, fully developed profiles at  $z/D = 100$  and  $150$  are in excellent agreement with the modified model predictions. The  $U$  velocity profiles for a smaller swirl number,  $S = 0.5$ , which was also investigated, were found to be very similar to the developing pipe flow with no swirl.

The decay of the tangential velocity is presented in Fig. 3. The measurements show that the locus of the maximum  $W$  velocity starts close to the wall at the inlet plane and then moves toward the symmetry axis further downstream, whereas the computations based on the two turbulence models maintain this locus at a pipe radius of about  $0.15$  from the wall. In general, the predictions based on the modified turbulence model show slower decay of the  $W$  profiles as compared with the results obtained using the standard model. At the same time, both sets of computations show slow decay of swirl when compared with the measurements. Overall, both models clearly exhibit a tendency to produce solid-body rotation, which is indicative of excessive radial diffusive transport.

Figure 4 illustrates profiles of the turbulence kinetic energy (nondimensionalized by  $U_\tau^2$ , where  $U_\tau$  is the friction velocity evaluated at  $z/D = 160$ ) for  $S = 1.445$ . Even though the case with  $S = 0.5$  is not presented, the conclusions pertaining to it are also discussed here. The computations are compared with measurements at four stations ( $z/D = 5.1, 10, 50$ , and  $150$ ). The experimental inlet conditions ( $z/D = 0.35$ ) are also included in Fig. 4. For the two swirl numbers investigated ( $S = 0.5$  and  $1.445$ ), the modified turbulence model consistently gives profiles below those predicted using the standard  $k-\epsilon$  model. The comparison of the experimental results with both sets of computations was good for the low swirl number ( $S = 0.5$ ). On the other hand, the agreement deteriorates for the higher swirl number ( $S = 1.445$ ), which is also shown in Fig. 4. This is clearly evident at the  $z/D = 50$  station, close to the symmetry axis. Similar findings are well documented for swirling flows, where nonisotropic effects are present and turbulence models based on an isotropic eddy viscos-

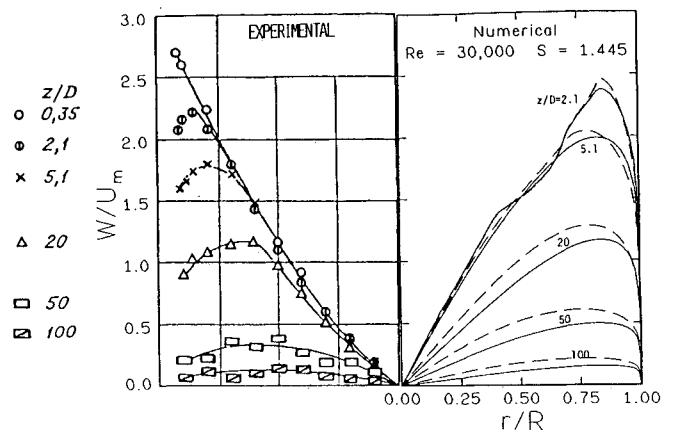


Fig. 3 Mean tangential velocity profiles.

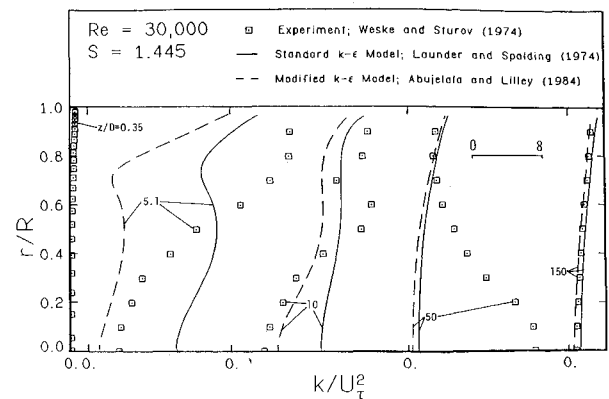


Fig. 4 Profiles of turbulent kinetic energy.

ity are not capable of resolving such complex phenomena. It was observed<sup>3</sup> that the modified  $k-\epsilon$  model gives dissipation levels higher than those obtained with the standard  $k-\epsilon$  model, primarily due to the enhancement of the source term in the  $\epsilon$  equation (alteration of  $C_2$ ).

### Conclusions

1) The trends and extent of the decaying tangential velocity in turbulent pipe flow are well predicted by the standard  $k-\epsilon$  model. The modified turbulence model results in slower decay as compared with the standard model, with no substantial improvement. Both models tend to produce solid-body rotation.

2) The comparison of the measured and computed turbulence kinetic energy profiles is very good for the low swirl number ( $S = 0.5$ ), whereas the agreement deteriorates for the higher swirl number ( $S = 1.445$ ).

### Acknowledgment

The authors acknowledge the financial support of the University of Illinois at Urbana-Champaign.

### References

- <sup>1</sup>Weske, D. R. and Sturov, G. Ye., "Experimental Study of Turbulent Swirled Flows in a Cylindrical Tube," *Fluid Mechanics: Soviet Research*, Vol. 3, 1974, pp. 77-82.
- <sup>2</sup>Patankar, S. V., *Numerical Heat Transfer and Fluid Flow*, Hemisphere, Washington, DC, 1980.
- <sup>3</sup>Khodadadi, J. M., "An Experimental and Numerical Investigation of Confined Coaxial Turbulent Jets," Ph.D. Thesis, Dept. of Mechanical and Industrial Engineering, Univ. of Illinois at Urbana-Champaign, Urbana, IL, 1986.
- <sup>4</sup>Lauder, B. E. and Spalding, D. B., "The Numerical Computation of Turbulent Flows," *Computer Methods Applied Mechanics Engineering*, Vol. 3, 1974, pp. 269-289.
- <sup>5</sup>Abujelala, M. T. and Lilley, D. G., "Limitations and Empirical Extensions of the  $k-\epsilon$  Model as Applied to Turbulent Confined Swirling Flows," *Chemical Engineering Communications*, Vol. 31, 1984, pp. 223-236.
- <sup>6</sup>Khodadadi, J. M. and Vlachos, N. S., "Experimental and Numerical Study of Confined Coaxial Turbulent Jets," *AIAA Journal*, Vol. 27, 1989, pp. 532-541.

## Boundary Layers for the Conical Navier-Stokes Equations

M. L. Rasmussen\* and Bok-Hyun Yoon†  
University of Oklahoma, Norman, Oklahoma

### Introduction

THE so-called conical Navier-Stokes (N-S) equations are a simplified set of equations that greatly reduce the complexity of numerical computations.<sup>1</sup> The equations are appropriate for studying viscous flows that have truly conical inviscid-flow counterparts, such as supersonic flows past cones and delta wings. They are also useful for generating starting solutions for more complicated parabolized Navier-Stokes computation schemes. Some of the earliest computations were undertaken by McRae<sup>2</sup> and Bluford,<sup>3,4</sup> and current studies also utilize the conical-flow approximation.<sup>5,6</sup> These results show overall good agreement with experimental results and other more complicated numerical schemes. However, it has been noticed that, especially for the thick viscous layers on the leeward side of inclined cones, the conical-approximation results show somewhat thinner boundary layers than indicated by experiment.<sup>2</sup> These discrepancies were attributed to non-conical nose effects associated with the experiments. However, it can be shown for axisymmetric flow that at least the conical N-S equations produce thinner boundary layers than the complete N-S counterparts. Thus it is a shortcoming of the conical N-S equations themselves that their associated boundary layers are too thin. It is the purpose of this Note to demonstrate these results for the simple case of axisymmetric flow.

### Formulation

We consider the simplest case, i.e., viscous axisymmetric supersonic flow past a circular cone (Fig. 1). In general, the flow variables depend on the polar coordinates  $r$  and  $\theta$ . Viscous effects prevail within the boundary layer along the cone surface ( $\theta = \theta_c$ ), in the very thin structure of the shock wave, and in the nose region where  $r$  is sufficiently small. In the inviscid region between the boundary layer and the shock, the flow is truly conical, and here the flow variables are functions of  $\theta$  only.

For the conical N-S equations, it is assumed that the flow variables for the viscous problem also depend on  $\theta$  only, or, more precisely, that their derivatives with respect to  $r$  can be ignored. This is essentially an irrational approximation because the  $r$  derivatives of the dependent variables are omitted arbitrarily. The coordinate  $r$  still remains in the viscous problem by virtue of the metric scale factors, but it appears only as a parameter and not as a participant in the differentiation on the dependent variables. For the axisymmetric flow case, therefore, only ordinary differential equations involving the polar angle  $\theta$  occur.

To set up the problem, we denote the  $r$  and  $\theta$  components of velocity by  $u$  and  $v$  and assume that the pressure  $p$ , density  $\rho$ , and temperature  $T$  are governed by a thermally and calorically perfect gas. Furthermore, we assume that the solution to the associated inviscid problem is known, and we denote the variables for the inviscid solution evaluated at the cone surface  $\theta_c$  by the subscript  $e$ . We shall use these inviscid values to normalize the viscous-flow variables. Thus we introduce the following normalized variables:

$$\begin{aligned} u/u_e &\rightarrow u, & v/v_e &\rightarrow v \\ p/p_e &\rightarrow p, & \rho/\rho_e &\rightarrow \rho, & T/T_e &\rightarrow T \\ \mu/\mu_e &\rightarrow \mu, & \lambda/\mu_e &\rightarrow \lambda \end{aligned} \quad (1)$$

Here  $\mu$  and  $\lambda$  are the first and second coefficients of viscosity. To complete the normalization process, we need the nondimensional parameters

$$\epsilon \equiv \frac{\mu_e}{\rho_e u_e r} \quad (2a)$$

$$Pr \equiv \frac{\mu_e c_p}{k} \quad (2b)$$

$$K_1 \equiv \frac{p_e}{\rho_e u_e^2} \quad (2c)$$

$$K_2 \equiv \frac{c_p T_e}{u_e^2} \quad (2d)$$

where  $c_p$  is the constant-pressure specific heat and  $k$  the thermal conductivity. We identify  $\epsilon$  as an inverse characteristic Reynolds number and  $Pr$  as the Prandtl number (assumed

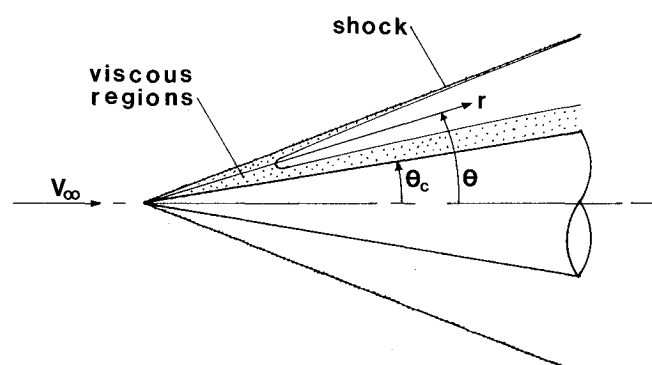


Fig. 1 Schematic for axisymmetric flow past a cone.

Received Feb. 13, 1989; revision received May 22, 1989. Copyright © 1989 American Institute of Aeronautics and Astronautics, Inc. All rights reserved.

\*Professor, Aerospace and Mechanical Engineering Department. Associate Fellow AIAA.

†Graduate Student, Aerospace and Mechanical Engineering Department.